A Chemical Transport Model Emulator for the Interactive Evaluation of Mercury Emission Reduction Scenarios

Francesco De Simone [1,*], **Francesco D'Amore** [1], **Francesco Marasco** [2], **Francesco Carbone** [1], **Mariantonia Bencardino** [1], **Ian M. Hedgecock** [1], **Sergio Cinnirella** [1], **Francesca Sprovieri** [1] and **Nicola Pirrone** [1]

[1] CNR-Institute of Atmospheric Pollution Research, Division of Rende, UNICAL Polifuzionale, 87036 Rende (CS), Italy; damore@iia.cnr.it (F.D.); carbone@iia.cnr.it (F.C.); bencardino@iia.cnr.it (M.B.); hedgecock@iia.cnr.it (I.M.H.); cinnirella@iia.cnr.it (S.C.); sprovieri@iia.cnr.it (F.S.); pirrone@iia.cnr.it (N.P.)

[2] Independent Researcher, via Picardi, 87100 Cosenza (CS), Italy; fmarasco@gmail.com

* Correspondence: francesco.desimone@iia.cnr.it

Abstract: Implementation of the Minamata Convention on Mercury requires all parties to "control, and where feasible, reduce" mercury (Hg) emissions from a convention-specified set of sources. However, the convention does not specify the extent of the measures to be adopted, which may only be analysed by decision-makers using modelled scenarios. Currently, the numerical models available to study the Hg atmospheric cycle require significant expertise and high-end hardware, with results which are generally available on a time frame of days to weeks. In this work we present HERMES, a statistical emulator built on the output of a global Chemical Transport Model (CTM) for Hg (ECHMERIT), to simulate changes in anthropogenic Hg (Hg_{anthr}) deposition fluxes in a source-receptor framework, due to perturbations to Hg_{anthr} emissions and the associated statistical significance of the changes. The HERMES emulator enables stakeholders to evaluate the implementation of different Hg_{anthr} emission scenarios in an interactive and real-time manner, simulating the application of the different Best Available Technologies. HERMES provides the scientific soundness of a full CTM numerical framework in an interactive and user-friendly spreadsheet, without the necessity for specific training or formation and is a first step towards a more comprehensive, and integrated, decision support system to aid decision-makers in the implementation of the Minamata Convention.

1. Introduction

Mercury (Hg) is a global pollutant since it impacts regions and ecosystems which are far from emission sources, due to its long range atmospheric transport [1]. The Minamata Convention on Mercury (MCM) (http://www.mercuryconvention.org/) was established to reduce mercury contamination resulting from anthropogenic activities. However, no specifications were set within the convention regarding policy and technical aspects, specific emission limits, reduction targets, or the specific control technologies to be applied [2,3].

Thus, each of the countries involved will apply their own measures unilaterally. However, it is clear that Hg pollution is a global concern, and a number of studies indicate that a coordinated set of actions is required for Hg emission control to be effective, due to the large uncertainties regarding the

processes that determine the global atmospheric cycle of Hg, and thus in establishing Source-Receptor (SR) relationships [4–6].

Selin [3], following the metric-based approach used in the context of the Montreal Protocol, to reduce halogens in the stratosphere [7], developed a metric that could be useful for policies focusing on the reduction of Hg pollution under the MCM.

The metric, however, as recognised by the authors, suffers from limitations since it was designed to capture the anthropogenic Hg, (hereafter Hg_{anthr}), contribution to global deposition, and therefore does not support any strategic policies focusing on reducing Hg_{anthr} deposition in a particular nation or region. It was also not designed to account directly for the emission speciation of Hg_{anthr}, which influences the fraction of Hg_{anthr} that deposits locally and/or regionally. This is a major limitation within the scope of current emission reduction strategies. Indeed, each of the Best Available Technologies (BATs) and Best Environmental Practices (BEPs) to be considered for reducing Hg_{anthr} emissions will result in a change of emission speciation [8], and therefore on the ratio of local to nonlocal Hg_{anthr} deposition. Furthermore, it does not provide information concerning the statistical significance of the outcome of any given reduction approach, which is necessary when facing the significant degree of uncertainty in modelling the processes related to Hg cycle in the different ecosystem compartments [4,5,9–12].

It is worth noting that the only available tools capable of tracking the fate of Hg_{anthr} from emission source to deposition receptor are Chemical Transport Models (CTMs) developed specifically to study the atmospheric cycle of Hg. Unfortunately, these complex numerical models require suitable expertise, specific training, and dedicated hardware to run. Even if packaged to be as user-friendly as possible, each run could require from hours to days for its entire workflow (design, initialisation, run, and results collection, analysis, and visualisation) to be completed, making them far from interactive, and unlikely to be used directly by policy-makers. Furthermore, a significant number of runs are required to provide statistically robust results. Clearly a simpler approach, directly accessible to policy-makers is required, to aid understanding and assessment of the Hg cycle and the implications of the policy options available. HERMES is an emulator built on an appropriate set of outputs obtained from the state-of-the-art Hg-CTM ECHMERIT [13,14].

Emulators are often used to simulate complex phenomena like climate change, (see, for example, Holden et al. [15], Castruccio et al. [16]) that permit the investigation of the forcing of arbitrary CO_2 concentrations on climate variables of interest at a computational cost that is many orders of magnitude lower than that required by a conventional climate model. Recent studies have applied the same basic principle to predict the response of O_3 and $PM_{2.5}$ concentrations to precursor emissions [17,18]. Other studies offer different statistical approaches used to increase the information from a limited set of model runs to investigate the uncertainty within processes simulated by conventional CTMs (see for example Beddows et al. [19]). However, none of these have been applied to the analysis of Hg pollution.

The output from HERMES allows the evaluation of the short-term (nominally one-year) effects on Hg_{anthr} deposition fluxes due to Hg_{anthr} emission perturbation. To cover a wide range of scenarios, in this work perturbations cover both emission reduction percentage and speciation, simulating the effect and the benefits of the BATs available to policy-makers for reducing Hg_{anthr} emissions, within a source-receptor framework [4].

With HERMES, a nonexpert user can perturb the Hg_{anthr} emissions in up to 15 source regions worldwide and can observe, in real-time, the effects on 21 receptor regions, and in particular with an indication of the statistical significance of the perturbation effects, relative to coefficient intervals of deposition as calculated in the current situation [4]. This aspect is of particular importance since it is necessary for researchers moving forward to increase transparency in order to inform policy makers of the limitations and uncertainties of the models used [20].

This approach overcomes the major issues identified in the prior state-of-the-art, allowing the evaluation of a number of emission reduction policy scenarios at the level of a specified region/country, as demonstrated in the following sections.

2. Materials and Methods

The basic idea behind the development of a CTM emulator is to run a number of anthropogenic emission control scenarios (the "Scenario experiments" below) and to analyse the response of the system in order to find a predictable pattern [17,18]. If such a pattern exists, it can be used to simulate the response of the system for all other possible emission scenarios, thus saving time and computational costs, within errors which magnitudes clearly depend on the goodness of fitting model used to approximate the response function.

2.1. Simulation of the Hg_{anthr} Atmospheric Cycle

The simulation of the atmospheric cycle of Hg_{anthr} was performed using the global Hg-CTM model ECHMERIT [13,14].

Two sets of experiments were conducted, where Hg_{anthr} emissions were tagged according to their source region, as reported in the HTAPv2 experiment (http://www.htap.org/) (see Figure 1), to allow the source apportionment of the subsequent Hg_{anthr} deposition. The Hg_{anthr} emissions were included in the model from three different anthropogenic inventories, referred to here as AMAP [21], EDGAR [22], and STREETS [23,24].

Firstly, the emission fields were mapped to the HTAPv2 mask at their original resolution using the large fraction area method, they were then interpolated onto the ECHMERIT T42 horizontal grid (roughly 2.8° by 2.8° at the equator) using the mass conserving remapping method; both methods are available in the Climate Data Operators (CDO) [25] package. Finally, the emissions were distributed vertically (up to 10 hPa), at run time, using the relevant prescribed height distribution, mapping them to Standardized Nomenclature for Air Pollutants (SNAP) and using the distribution in Simpson et al. [26] or evenly injecting them within the Planetary Boundary Layer (PBL) (see De Simone et al. [10] for details).

A spin-up period of 4 years was employed for both sets of runs, and the results from the fifth year, namely 2010, were then considered for the analysis.

A BASE run is shared by both sets of experiments and includes an Hg oxidation mechanism driven by O_3/OH fields, imported from the Mozart model [27], and Hg_{anthr} emissions from AMAP/UNEP [21].

The first set of experiments, the "Characterising experiments", aims only to define and characterise the Hg_{anthr} atmospheric cycle to provide robust constraints of confidence intervals of the contributions to deposition in each receptor region. To this aim, a number of parameters, model assumptions, and inventories were varied, covering a reasonable range of uncertainties known to influence the Hg atmospheric cycle. All these runs, although leading to changes in Hg surface concentration and deposition fields, were demonstrated to be statistically indistinguishable between each other when compared with the available field measurements, as described in [10].

A number of runs were conducted employing different Hg_{anthr} emission height distributions (APBL), as well as different Hg_{anthr} speciation ratios, only as $Hg^0_{(g)}$ (NSP0), or emitted at a ratio $Hg^0_{(g)}$:$Hg^{II}_{(g/p)}$ 50/50 (NSP50).

Years with different meteorological characteristics were also simulated to evaluate the effects of changing atmospheric transport conditions, (BASE-2005 and BASE-1998). They were selected according to opposite values of major climatic indices which result in different circulation and precipitation patterns [28,29].
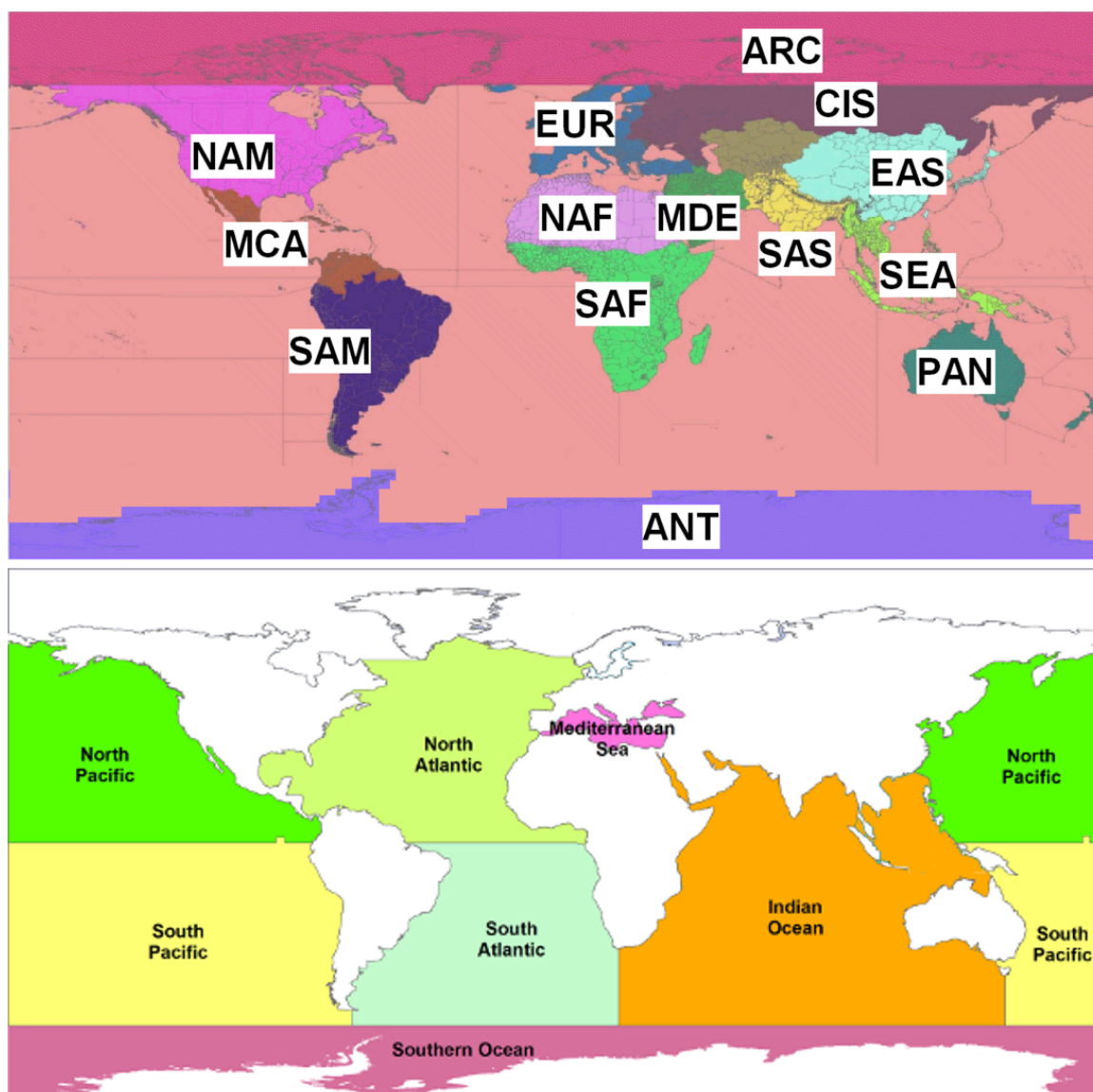
Figure 1. Upper panel: definition of the source regions used herein. NAM (North America), EUR (Europe), SAS (South Asia), EAS (East Asia), SEA (South East Asia), PAN (Australia), NAF (North Equatorial Africa), SAF (South Equatorial Africa), MDE (Middle East Asia), MCA (Central America), SAM (South America), CIS (Central Asia), ARC (Arctic, above 66° N). Lower panel: Definition of the ocean basins used here. Note that Southern Ocean and ANT are, respectively, the ocean and the Antarctic continent below 60° S.

Due to uncertainties of the atmospheric Hg oxidation pathway [30–32], a run was performed considering an oxidation mechanism based on Bromine (BRTO) (from p-Tomcat [33,34]).

Finally, two runs including, respectively, EDGAR and STREETS inventories were run to explicitly account for the uncertainties regarding Hg_{anthr} emissions.

A summary of the runs performed within the scope of the Characterising experiments is reported in Table 1 below.

Table 1. "Characterising experiments" that computed the Hg_{anthr} deposition in each receptor region.

Run	Inventory	Ref. Year	Meteor. Year	Speciation	Vertical Profile	Oxidation
BASE	AMAP-2010	2010	2010	Native	Native	O_3+OH
BASE-2005	AMAP-2010	2010	2005	Native	Native	O_3+OH
BASE-1998	AMAP-2010	2010	1998	Native	Native	O_3+OH
APBL	AMAP-2010	2010	2010	Native	Uniform PBL	O_3+OH
NSP0	AMAP-2010	2010	2010	as $Hg_{(g)}^0$	Native	O_3+OH
NSP50	AMAP-2010	2010	2010	$Hg_{(g)}^0$:$Hg_{(g)}^{II}$ = 50:50	Native	O_3+OH
BRTO	AMAP-2010	2010	2010	Native	Native	Bromine
STREETS	STREETS	2010	2010	Native	Uniform PBL	O_3+OH
EDGAR	EDGAR	2010	2010	Native	Native-SNAP	O_3+OH

A bootstrap analysis [35] was then used to evaluate the average Hg_{anthr} deposition in each receptor region due to each source region and to determine the relative confidence intervals, following the procedure described in De Simone et al. [4].

The second set of experiments, defined as "Scenario experiments", represents the core of the present study. The runs belonging to this set were performed using only the AMAP/UNEP [21] emission inventory, since for the scope of this study we want to simulate the response of Hg_{anthr} deposition to Hg_{anthr} emission perturbations using this inventory.

To simplify the emission control simulations, we assumed a decrease of the number of Hg_{anthr} species emitted. Gaseous elemental mercury ($Hg_{(g)}^0$) and reactive mercury (Hg^R) were taken into account. The latter as a lumped species representing oxidised mercury ($Hg_{(g)}^2$) and particle bounded mercury $Hg_{(p)}$, both considered to be emitted with a constant ratio as in AMAP/UNEP [21]. Reduction changes were simulated (BaseR20 to BaseR80), as were different ratios of $Hg_{(g)}^0$:Hg^R (BaseS00 to BaseS100), leaving all other model parameters and assumptions equal to those in the BASE run. The runs of Scenario experiments, listed in Table 2, were used to build the HERMES emulator, as described in the following Section 2.2.

Table 2. List of Scenario experiments conducted with a common emission database (AMAP [21]) and reducing the emissions (BaseR20 to BaseR80) as well as changing the speciation ratio (BaseS00 to BaseS100).

Run	Emissions	HgR:Hg0	Reduction
BASE	AMAP	Original	None
BaseR20	AMAP	Original	20%
BaseR40	AMAP	Original	40%
BaseR60	AMAP	Original	60%
BaseR80	AMAP	Original	80%
BaseS00	AMAP	0:100	None
BaseS20	AMAP	20:80	None
BaseS40	AMAP	40:60	None
BaseS60	AMAP	60:40	None
BaseS80	AMAP	80:60	None
BaseS100	AMAP	100:0	None

2.2. Building the HERMES Emulator

The scope of this study is to provide a CTM emulator, HERMES, to calculate new Hg_{anthr} deposition fluxes for each receptor related to Hg_{anthr} emission perturbation(s) in one or more source regions. The characteristics of the Hg_{anthr} emission amount and speciation ratio, can be controlled, thus simulating the adoption of available abatement techniques. The HERMES emulator output is a new Hg_{anthr} deposition value for each receptor. To achieve this, the deposition fields resulting from the Scenario experiment ECHMERIT runs were fitted using the best model available.

Since Hg in the CTM model is due only to the anthropogenic emissions (i.e., Hg_{anthr} species are neither created nor destroyed within the model), the deposition in the model domain cells resulting from Hg_{anthr} emission reduction (runs BaseR20 to BaseR80) is directly proportional to the reduction (adjusted $R^2 \sim 1$). Therefore, the Hg_{anthr} deposition in the receptor region r due to the emission reduction in the source region s, namely $DEP_{r,s}^{Red}$, is calculated by HERMES as follows

$$DEP_{r,s}^{Red} = (100 - INPUT_s^{Red}) * DEP_{r,s}^{BASE} \tag{1}$$

where $INPUT_s^{Red}$ is the Hg_{anthr} emission reduction in the source region s as a percentage (0–100%), and $DEP_{r,s}^{BASE}$ is the Hg_{anthr} deposition, in the receptor region r due to the source region s, in the unperturbed scenario (BASE run).

A linear model is also sufficient (adjusted $R^2 \sim 1$) to describe the Hg_{anthr} deposition resulting from emission speciation perturbation runs(BaseS00 to BaseS100) and Hg_{anthr} deposition in the receptor region r due to the emission speciation perturbation in the source region s, $DEP_{r,s}^{Spec}$, is,

$$DEP_{r,s}^{Spec} = A_{s,r}^{Spec} + INPUT_s^{Spec} * B_{s,r}^{Spec} \tag{2}$$

where $INPUT_s^{Spec}$ represents the ratio between $Hg_{(g)}^0$ (0 = 100%) and Hg^R (1 = 100%); $A_{s,r}^{Spec}$ and $B_{s,r}^{Spec}$ are the coefficients of the linear equation and represent the deposition of Hg_{anthr} in the receptor region r due to the emission in source region s in the case where Hg_{anthr} is totally gaseous and the rate at which the deposition changes as the contribution of reactive mercury increases.

From relation (1) between $DEP_{r,s}^{Red}$ and $INPUT_s^{Red}$, the following polynomial can be derived relating the deposition $DEP_{r,s}^{HERMES}$, in the receptor region r due to the change of Hg_{anthr} in both terms of emission reduction ($INPUT_s^{Rec}$), and speciation ($INPUT_s^{Spec}$) in the source region s:

$$DEP_{r,s}^{HERMES} = A_{s,r}^{Spec} * (100 - INPUT_s^{Red}) + INPUT_s^{Spec} * B_{s,r}^{Spec} * (100 - INPUT_s^{Red}) \tag{3}$$

with all variables as defined above.

Equation (3) represents the core of the of HERMES emulator, and for ease of use it is implemented in a spreadsheet file available in the Supporting Information.

The new deposition value, $DEP_{r,s}$, is finally compared to the relative bounds at 95% confidence interval (CI) at either tail (see Table 3), with indications if it falls outside the bounds, as further described below.

By the way the experiments were designed, the HERMES emulator calculates the $DEP_{r,s}^{HERMES}$, in the receptor region r due to the perturbation(s) of Hg_{anthr} emission in the source region s, nominally after one year following the emission perturbation(s).

Moreover, since we included for this analysis only the Hg emissions from anthropogenic activities, Equations (1) and (2) represent processes that are perfectly linear, as demonstrated by a number of tests regarding the goodness of fit (adjusted $R^2 \sim 1$, residuals plots and significance of model regression test based on ANOVA at $\alpha = 0.01$). The equations fit perfectly the response of the Hg_{anthr} deposition to control scenarios of Hg_{anthr} emissions, in terms of reduction and speciation, respectively, and therefore, they must not be regarded as simple linearisation of the response function.

Since the core Equation (3) is a simple combination of Equations (1) and (2), it means that HERMES can simulate the output of any ECHMERIT runs actually without errors. Indeed, the only differences are negligible, in the order of Kgs, and are just due to the numerical or computational errors in CTM sampling and/or fitting algorithm.

Table 3. Reference (BASE), and upper and lower bound (95% level) for the mean of the Hg$_{anthr}$ total deposition (Mg/year) for each receptor region originating from all source regions.

Region	Lower Bound	Reference	Upper Bound
North America	66.87	78.41	87.96
Australia	12.86	16.08	18.97
South East Asia	117.68	146.08	182.35
Europe	30.60	37.11	43.21
Indonesia	21.21	25.15	28.39
Arctic	32.46	35.95	38.85
Central America	20.12	23.44	26.31
Middle East Asia	15.42	17.65	19.35
North Equatorial Africa	33.61	41.56	59.13
Central Asia	69.35	79.56	89.37
South Equatorial Africa	74.47	89.35	101.95
South America	55.27	65.89	74.82
South Asia	34.50	45.87	57.75
Antarctic	2.60	4.34	7.26
Ocean Basins	**Lower Bound**	**Reference**	**Upper Bound**
North Atlantic	143.15	159.07	168.66
South Atlantic	90.73	109.85	125.38
North Pacific	392.65	440.93	471.62
South Pacific	230.59	278.56	316.00
Indian	163.22	197.70	223.76
Mediterranean	7.87	9.05	10.33
South Ocean	8.35	11.17	15.25

3. Results

The outcomes of the Characteristic experiments are summarised in Table 3. It shows, for each of the receptor regions, the reference Hg$_{anthr}$ deposition (Mg/year) due to all of the source regions, as calculated by the BASE run ($\sum_s DEP_r^{BASE}$). Moreover, it reports the upper and lower bound of the confidence interval (at a 95% level) of the mean of the Hg$_{anthr}$ total deposition (Mg/year), due to all the source regions, as estimated by bootstrap.

3.1. HERMES Case Studies

Figure 2 illustrates the implementation of HERMES emulator in a spreadsheet and reported in SI.

The upper-left Section (1 in green) shows the input window in which each source region is provided with two sets of sliding bars to change Hg$_{antrh}$ emission for each of the source regions. The first slider can reduce the emissions as a percentage, whereas the second allows the selection of the ratio between elemental and reactive Hg$_{antrh}$.

The right section of the figure illustrates the output list of receptors, for both terrestrial (2 in orange) and oceanic (3 in light blue) receptors, each one provided with its reference value, the newly calculated value, and the percentage change of the Hg$_{antrh}$ deposition. As explained before, the output is considered nominally one year following Hg$_{anthr}$ emission perturbation. Two columns are also reported that are normally blank. The cells eventually become green (or red) if the deposition decrease (or increase) is statistically significant (at a 95% level of confidence).

A summary reports total deposition over terrestrial and oceanic receptors.

The lower-left Section (4 in yellow) reports in a graphical form the results for terrestrial and oceanic regions. Perturbed deposition fluxes (red bars) are compared against the reference deposition (blue bars) for each receptor.

A reset button returns emission changes to zero (BASE case).
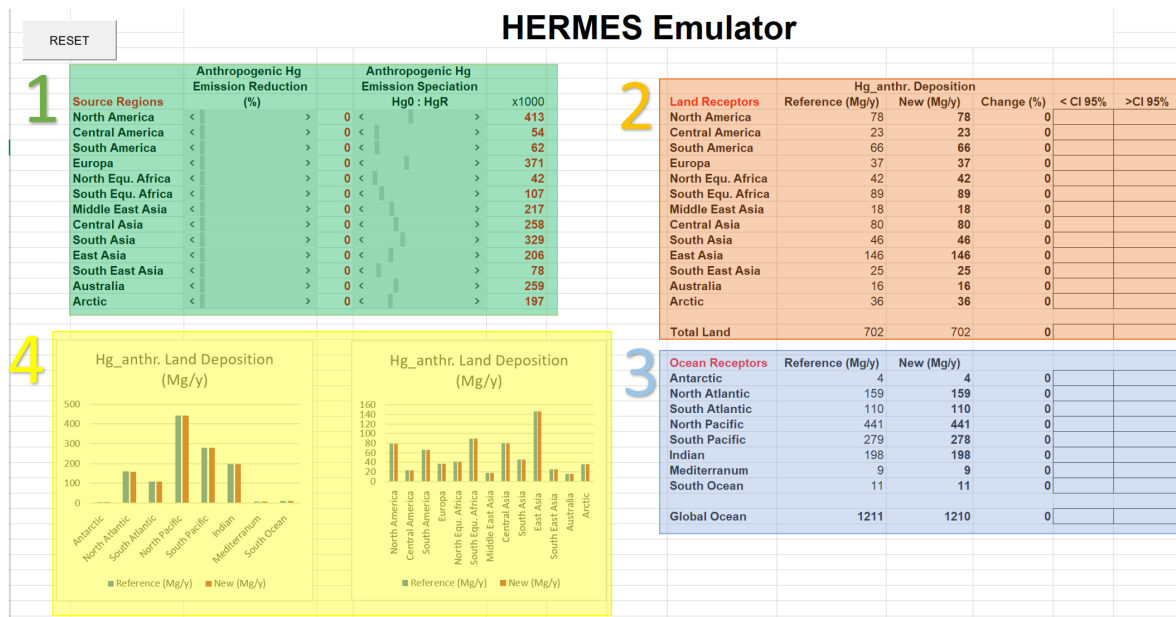
Figure 2. Dashboard interface of HERMES emulator implemented in a spreadsheet with input Section (1, in green), numerical output Sections (2 and 3, orange and light blue), and graphical output Section (4, in yellow).

3.2. Hg Emission Reduction

To show the potential of HERMES to support decision-makers, a number of case studies are reported hereafter. The first portfolio of cases is related to Hg_{anthr} emission reduction.

3.2.1. Emissions—20% in all Source Regions

If we reduce by 20% the Hg_{anthr} emission in all source regions (Figure 3) we see a 20% reduction of deposition in each receptor. In all receptors the change in deposition is effective (green cells) except for the South Asia, Southern Oceans, and Antarctic, where the uncertainty in the deposition is so high that a 20% in reduction is not of statistical significance [4].
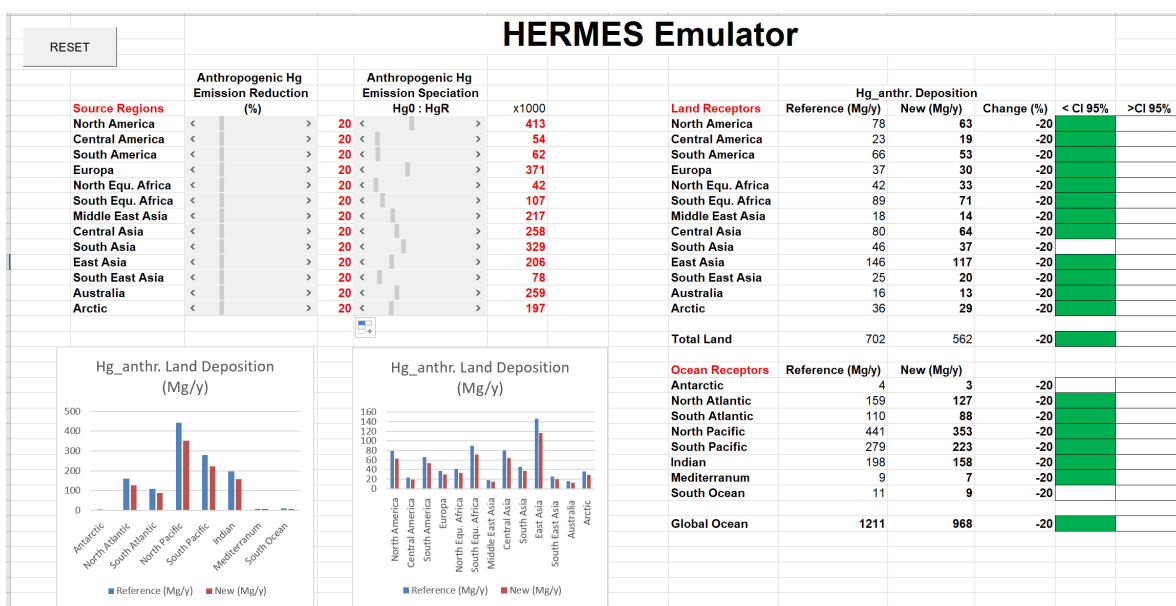
Figure 3. Use-case 1: Hg_{anthr} emission reduction by 20% from all source regions.

3.2.2. Emissions—50% in Key Regions: Europe, East Asia, and North America

In the next example cases we test the effects of reducing by 50% the Hg_{anthr} emissions in some key source regions to help decision-makers evaluate the extent of eventual measures applied to single countries. When applied to Europe, Figure 4, this measure results in a significant decrease over Europe itself (−26%) and the nearby Mediterranean sea (−17%), whereas the effects over other receptors, although measurable, are not significant.

HERMES Emulator

Source Regions	Anthropogenic Hg Emission Reduction (%)	Anthropogenic Hg Emission Speciation Hg0 : HgR	x1000	Land Receptors	Hg_anthr. Deposition Reference (Mg/y)	New (Mg/y)	Change (%)	< CI 95%	>CI 95%
North America	0	0	413	North America	78	76	-3		
Central America	0	0	54	Central America	23	23	-2		
South America	0	0	62	South America	66	65	-2		
Europa	50	0	371	Europa	37	28	-26	■	
North Equ. Africa	0	0	42	North Equ. Africa	42	39	-6		
South Equ. Africa	0	0	107	South Equ. Africa	89	88	-2		
Middle East Asia	0	0	217	Middle East Asia	18	17	-4		
Central Asia	0	0	258	Central Asia	80	75	-6		
South Asia	0	0	329	South Asia	46	45	-1		
East Asia	0	0	206	East Asia	146	144	-1		
South East Asia	0	0	78	South East Asia	25	25	-2		
Australia	0	0	259	Australia	16	16	-2		
Arctic	0	0	197	Arctic	36	34	-5		
				Total Land	702	674	-4		

| Ocean Receptors	Reference (Mg/y)	New (Mg/y)	Change	< CI 95%	>CI 95%
Antarctic	4	4	-2		
North Atlantic	159	153	-4		
South Atlantic	110	108	-2		
North Pacific	441	429	-3		
South Pacific	279	273	-2		
Indian	198	194	-2		
Mediterranum	9	8	-17	■	
South Ocean	11	11	-2		
Global Ocean	1211	1181	-2		

Hg_anthr. Land Deposition (Mg/y)

Hg_anthr. Land Deposition (Mg/y)

Figure 4. Use-case 2: Hg_{anthr} emission reduction by 50% in Europe.

If we reduce by 50% the Hg_{anthr} emissions in East Asia (Figure 5), there is an evident and significant reduction in a number of regions resulting in an annual deposition decrease over oceans (16%) and land (18%). Due to the long-range transboundary transport of Hg_{anthr}, the reduction can impact the Americas, the Arctic, and the whole of Asia as well as the Atlantic Ocean. Reduction of deposition over regions ranges from 35% for East Asia to about 16% of Central America, the Middle East, and Central Asia. This measure has a great impact over the oceans of the Norther Hemisphere with a decrease of Hg_{anthr} deposition of 18% for the North Atlantic and 21% for the North Pacific.

Over other receptors, despite the decrease ranging from 9% for South Asia to 17% for North. Eq. Africa, it is not significant.

It is of interest how the reduction of Hg_{anthr} emissions by 50% in North America (Figure 6) has no significant effects in any of the receptor regions.

HERMES Emulator

Land Receptors	Reference (Mg/y)	New (Mg/y)	Change (%)
North America	78	65	-17
Central America	23	20	-16
South America	66	58	-12
Europa	37	33	-10
North Equ. Africa	42	34	-17
South Equ. Africa	89	78	-12
Middle East Asia	18	15	-16
Central Asia	80	67	-16
South Asia	46	42	-9
East Asia	146	95	-35
South East Asia	25	21	-15
Australia	16	14	-11
Arctic	36	29	-19
Total Land	702	572	-19

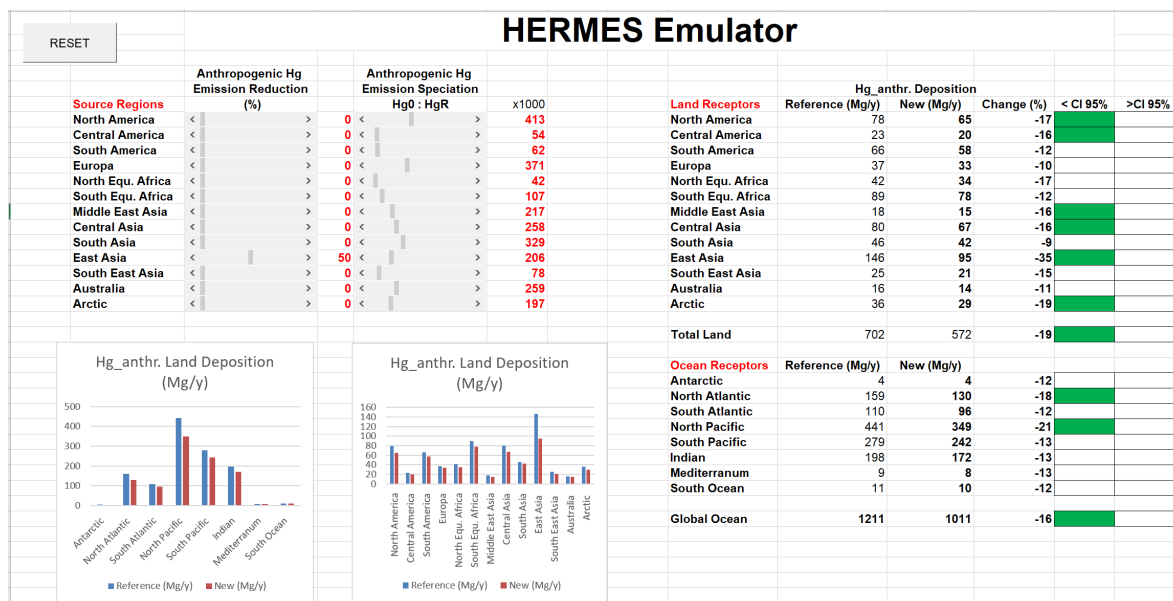| Ocean Receptors	Reference (Mg/y)	New (Mg/y)	Change (%)
Antarctic	4	4	-12
North Atlantic	159	130	-18
South Atlantic	110	96	-12
North Pacific	441	349	-21
South Pacific	279	242	-13
Indian	198	172	-13
Mediterranum	9	8	-13
South Ocean	11	10	-12
Global Ocean	1211	1011	-16

Figure 5. Use-case 3: Hg_{anthr} emission reduction by 50% in East Asia.

HERMES Emulator

Land Receptors	Reference (Mg/y)	New (Mg/y)	Change (%)
North America	78	71	-10
Central America	23	23	-2
South America	66	65	-1
Europa	37	37	-1
North Equ. Africa	42	41	-2
South Equ. Africa	89	88	-1
Middle East Asia	18	17	-2
Central Asia	80	78	-2
South Asia	46	46	-1
East Asia	146	145	-1
South East Asia	25	25	-1
Australia	16	16	-1
Arctic	36	35	-2
Total Land	702	687	-2

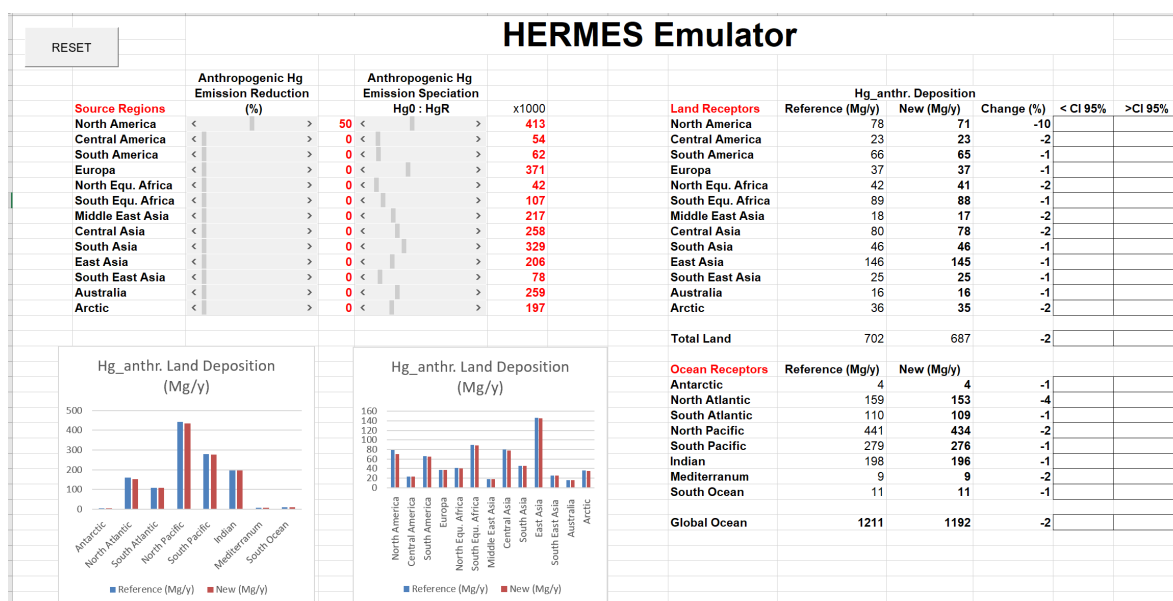| Ocean Receptors	Reference (Mg/y)	New (Mg/y)	Change (%)
Antarctic	4	4	-1
North Atlantic	159	153	-4
South Atlantic	110	109	-1
North Pacific	441	434	-2
South Pacific	279	276	-1
Indian	198	196	-1
Mediterranum	9	9	-2
South Ocean	11	11	-1
Global Ocean	1211	1192	-2

Figure 6. Use-case 4: Hg_{anthr} emission reduction by 50% in North America.

3.3. Hg Speciation Perturbation

Changes in Hg_{anthr} emission abatement strategies were tested by modifying the $Hg_{(g)}^{0}$:Hg^{R} ratio. Perturbation of this ratio does not affect the amount of Hg_{anthr} deposition on a global scale but only impacts its distribution, which may be of policy interest on a regional scale. For this case, we tested two contrasting scenarios: $Hg_{(g)}^{0} = 0$ and $Hg^{R} = 100$; and $Hg_{(g)}^{0} = 100$ and $Hg^{R} = 0$.

In the first scenario there is a greater fraction of Hg_{anthr} reaching the global pool (Figure 7), thereby tending to reduce deposition to the regions that are sources and increasing deposition over ocean basins. However, no single change is statistically significant for any of the receptors. In the second scenario, emissions have a shorter atmospheric residence time, resulting in deposition occurring closer to the emission sources (Figure 8). The distribution of Hg_{anthr} deposition among the receptors changes markedly also in this case. It increases over land and decreases over oceans, with the exception of the Mediterranean Sea where the deposition increases by 11%. However, only deposition changes over Europe and South East Asia are statistically significant, with an increase of 19% and 30%, respectively.
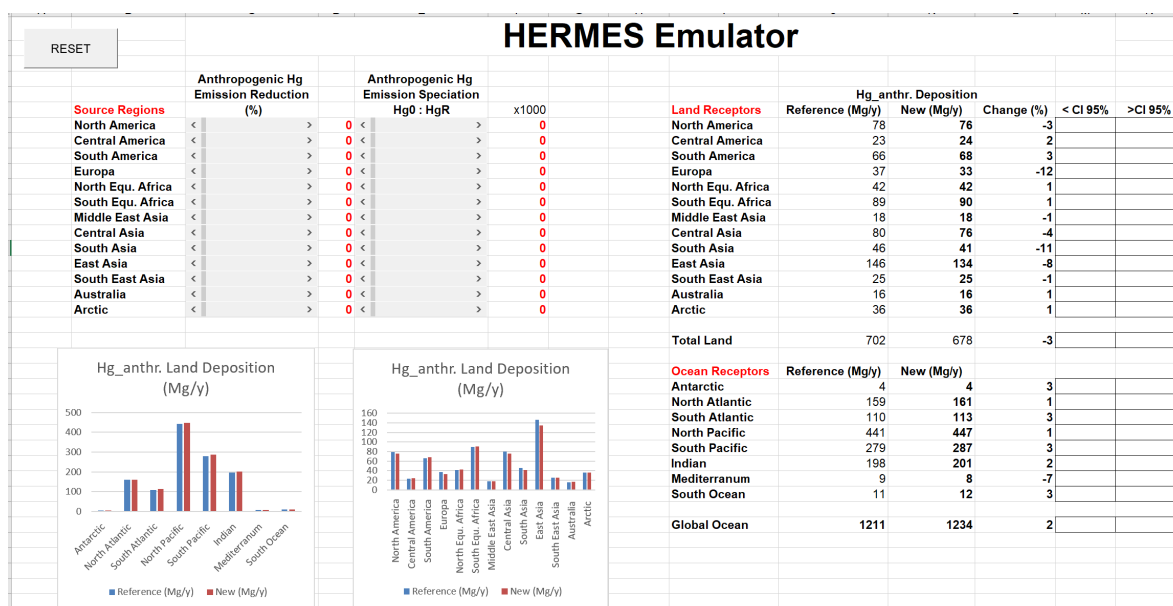
HERMES Emulator

Source Regions	Anthropogenic Hg Emission Reduction (%)				Anthropogenic Hg Emission Speciation Hg0 : HgR			x1000		Land Receptors	Hg_anthr. Deposition Reference (Mg/y)	New (Mg/y)	Change (%)	< CI 95%	>CI 95%
North America	<		>	0	<		>	0		North America	78	76	-3		
Central America	<		>	0	<		>	0		Central America	23	24	2		
South America	<		>	0	<		>	0		South America	66	68	3		
Europa	<		>	0	<		>	0		Europa	37	33	-12		
North Equ. Africa	<		>	0	<		>	0		North Equ. Africa	42	42	1		
South Equ. Africa	<		>	0	<		>	0		South Equ. Africa	89	90	1		
Middle East Asia	<		>	0	<		>	0		Middle East Asia	18	18	-1		
Central Asia	<		>	0	<		>	0		Central Asia	80	76	-4		
South Asia	<		>	0	<		>	0		South Asia	46	41	-11		
East Asia	<		>	0	<		>	0		East Asia	146	134	-8		
South East Asia	<		>	0	<		>	0		South East Asia	25	25	-1		
Australia	<		>	0	<		>	0		Australia	16	16	1		
Arctic	<		>	0	<		>	0		Arctic	36	36	1		
										Total Land	702	678	-3		
										Ocean Receptors	Reference (Mg/y)	New (Mg/y)			
										Antarctic	4	4	3		
										North Atlantic	159	161	1		
										South Atlantic	110	113	3		
										North Pacific	441	447	1		
										South Pacific	279	287	3		
										Indian	198	201	2		
										Mediterranum	9	8	-7		
										South Ocean	11	12	3		
										Global Ocean	1211	1234	2		

Figure 7. Use-case 5: Hg_{anthr} fully emitted as $Hg^0_{(g)}$ from all sources.

HERMES Emulator

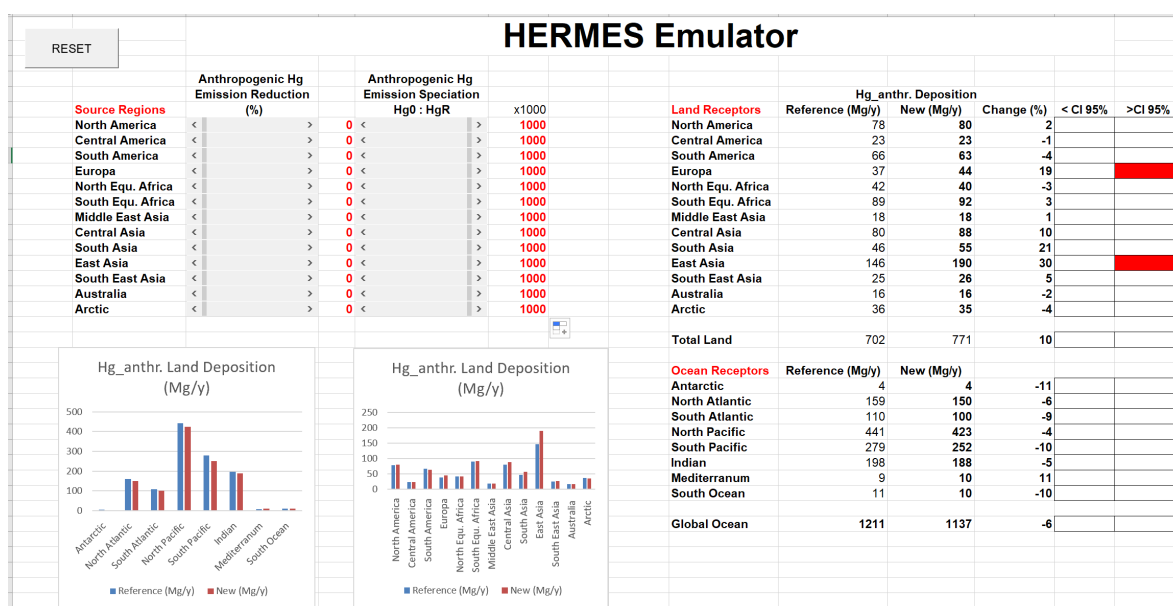| Source Regions	Anthropogenic Hg Emission Reduction (%)				Anthropogenic Hg Emission Speciation Hg0 : HgR			x1000		Land Receptors	Hg_anthr. Deposition Reference (Mg/y)	New (Mg/y)	Change (%)	< CI 95%	>CI 95%
North America	<		>	0	<		>	1000		North America	78	80	2		
Central America	<		>	0	<		>	1000		Central America	23	23	-1		
South America	<		>	0	<		>	1000		South America	66	63	-4		
Europa	<		>	0	<		>	1000		Europa	37	44	19		red
North Equ. Africa	<		>	0	<		>	1000		North Equ. Africa	42	40	-3		
South Equ. Africa	<		>	0	<		>	1000		South Equ. Africa	89	92	3		
Middle East Asia	<		>	0	<		>	1000		Middle East Asia	18	18	1		
Central Asia	<		>	0	<		>	1000		Central Asia	80	88	10		
South Asia	<		>	0	<		>	1000		South Asia	46	55	21		
East Asia	<		>	0	<		>	1000		East Asia	146	190	30		red
South East Asia	<		>	0	<		>	1000		South East Asia	25	26	5		
Australia	<		>	0	<		>	1000		Australia	16	16	-2		
Arctic	<		>	0	<		>	1000		Arctic	36	35	-4		
										Total Land	702	771	10		
										Ocean Receptors	Reference (Mg/y)	New (Mg/y)			
										Antarctic	4	4	-11		
										North Atlantic	159	150	-6		
										South Atlantic	110	100	-9		
										North Pacific	441	423	-4		
										South Pacific	279	252	-10		
										Indian	198	188	-5		
										Mediterranum	9	10	11		
										South Ocean	11	10	-10		
										Global Ocean	1211	1137	-6		

Figure 8. Use-case 6: Hg_{anthr} fully emitted as Hg^R from all sources.

4. Discussion and Further Development

In this paper we illustrated the HERMES emulator based on the ECHMERIT Hg-CTM [9–11] aimed to investigate the fate of Hg_{anthr} emissions over land and oceans. HERMES captures the essence of the complexity of the Hg cycle enabling the end-user to obtain interactive and real time results. It provides the full capability of a scientifically robust and validated model, which usually requires advanced scientific formation and technical skills to be used and high-end computing infrastructure to run. We demonstrate how the spreadsheet interface makes the manipulation of Hg_{anthr} emissions in each source region user-friendly, providing a tool for policy-makers that can be used to assess short-term effects (nominally one year) of the Hg_{anthr} emission perturbation (both reduction and speciation), in real-time and without any specific training or formation.

The linear relationships found for the response of Hg_{anthr} deposition to emissions control scenarios (Equations (1) and (2)) are due to the simplification of the inclusion of only Hg_{anthr} in the model.

The inclusion of other natural and legacy Hg emissions in the model is likely to introduce some nonlinearity. Indeed, because of the complexity of the Earth System, and the time scales involved, legacy Hg re-emissions or exchange of chemical compounds between environmental compartments are not captured by HERMES. However, the Hg_{anthr} deposition reduction to a specific ecosystem is an important first step in the reduction of the Hg burden in that particular ecosystem. In the future developments, a more complete CTM emulator could be built, including all Hg emission sources, depending on the computational trade-off between the number of emission control scenarios required and the goodness of the fit of the response function. In addition or alternatively, the proposed approach could be integrated with existing tools for the evaluation of long-term abatement strategies, by customising it to a source-receptor version of any biogeochemical cycle model, a number of which have been publicly released (see, for example [36]).

At this development stage, the reduction percentage and the speciation ratio provided for the Hg_{anthr} emissions in each source region affects all the emission sectors in that region. It is possible to overcome this simplification by explicitly considering different industrial sectors within each source region. This functionality will require multiple new model runs, but the computational effort would support decision-makers in implementing more precise reduction strategies for each emission sector in a given region. As a forward integration step, these strategies could be associated with their economic and social costs, in such a way the best solution, in terms of both environmental and economic costs, could be assessed.

The confidence intervals provided for Hg_{anthr} deposition over receptor regions are calculated starting from the ensemble of runs defined as, "Characterising experiments", as in previous work [4]. Although these runs consider a reasonable range of possible sources of uncertainty, they were designed to assess one source at a time and therefore they do not consider all the plausible combinations of uncertainties. This is due to the computational effort that would be required. Moreover, it should be noted that confidence intervals are calculated based on the current anthropogenic emissions, and therefore the statistical significance of the newly calculated deposition fields are related to the present situation. A more robust statistical comparison between new and present Hg deposition figures would require the calculation of confidence intervals for each of the runs belonging to "Scenario experiments", (i.e., the combination of runs belonging to the Characterising experiment and the Scenario experiment), and their relative comparison, which would require at least one order of magnitude more CTM runs. Although shortcomings exist, we believe that the comparison of the Hg_{anthr} deposition simulated by HERMES for a given scenario with the Hg_{anthr} deposition confidence intervals calculated considering the present situation is a reasonable starting point to try to establish an operational calculation of the statistical significance associated with any given policy measures to be adopted.

However, these shortcomings will be addressed in the future versions of HERMES, which are currently under development, that could be distributed on the Web, to further engage the user experience and to provide mechanically readable services in order to improve different user scenarios and interoperability between systems. The web portal of the next version of HERMES could be composed of several widgets with interactive graphs and data tables to provide improved data visualisation. In this way, HERMES would be able to reach multiple users and used more effectively, utilising the same tool, the web, to which stakeholders are accustomed.

5. Conclusions

In this study we presented HERMES, a statistical emulator built on the output of a Chemical Transport Model (CTM) for Hg (ECHMERIT), to simulate changes in Hg_{anthr} deposition fluxes due to perturbations to Hg_{anthr} emissions. The perturbations encompass both speciation and reduction, simulating thus the implementation of different Best Available Technologies. Hg_{anthr} deposition fluxes are calculated in a source-receptor framework, enabling the evaluation of the impact any specific Hg_{anthr} emission reduction scenario both regionally and globally, and provide the statistical significance

of the deposition flux changes, as compared with the current situation. HERMES provides the scientific soundness of a full CTM numerical framework in an interactive and user-friendly spreadsheet and does not require specific training or formation for use. HERMES is the core pillar of a more comprehensive, and integrated, decision support system to aid decision-makers in the evaluation of Hg$_{anthr}$ emission reduction policies taken under the Minamata Convention.

Abbreviations

The following abbreviations are used in this manuscript:

Hg$_{anthr}$	Hg emitted from anthropogenic activities
Hg	Hg circulating within the Earth System; Hg includes Hg$_{anthr}$
MDPI	Multidisciplinary Digital Publishing Institute
DOAJ	Directory of open access journals

References

1.　Fitzgerald, W.F.; Engstrom, D.R.; Mason, R.P.; Nater, E.A. The case for atmospheric mercury contamination in remote areas. *Environ. Sci. Technol.* **1998**, *32*, 1–7. [CrossRef]

2.　Selin, H.; Keane, S.E.; Wang, S.; Selin, N.E.; Davis, K.; Bally, D. Linking science and policy to support the implementation of the Minamata Convention on Mercury. *Ambio* **2018**, *47*, 198–215. [CrossRef] [PubMed]

3.　Selin, N.E. A proposed global metric to aid mercury pollution policy. *Science* **2018**, *360*, 607–609. [CrossRef] [PubMed]

4.　De Simone, F.; Hedgecock, I.M.; Carbone, F.; Cinnirella, S.; Sprovieri, F.; Pirrone, N. Estimating Uncertainty in Global Mercury Emission Source and Deposition Receptor Relationships. *Atmosphere* **2017**, *8*, 236. [CrossRef]

5.　Kwon, S.Y.; Selin, N.E. Uncertainties in atmospheric mercury modeling for policy evaluation. *Curr. Pollut. Rep.* **2016**, *2*, 103–114. [CrossRef]

6.　Gustin, M.S.; Evers, D.C.; Bank, M.S.; Hammerschmidt, C.R.; Pierce, A.; Basu, N.; Blum, J.; Bustamante, P.; Chen, C.; Driscoll, C.T.; et al. Importance of Integration and Implementation of Emerging and Future Mercury Research into the Minamata Convention. *Environ. Sci. Technol.* **2016**, *50*, 2767–2770. [CrossRef]

7.　Daniel, J.S.; Solomon, S.; Albritton, D.L. On the evaluation of halocarbon radiative forcing and global warming potentials. *J. Geophys. Res. Atmos.* **1995**, *100*, 1271–1285. [CrossRef]

8.　Giang, A.; Stokes, L.C.; Streets, D.G.; Corbitt, E.S.; Selin, N.E. Impacts of the minamata convention on mercury emissions and global deposition from coal-fired power generation in Asia. *Environ. Sci. Technol.* **2015**, *49*, 5326–5335. [CrossRef]

9.　De Simone, F.; Cinnirella, S.; Gencarelli, C.N.; Yang, X.; Hedgecock, I.M.; Pirrone, N. Model study of global mercury deposition from biomass burning. *Environ. Sci. Technol.* **2015**, *49*, 6712–6721. [CrossRef]

10.　De Simone, F.; Gencarelli, C.N.; Hedgecock, I.M.; Pirrone, N. A modeling comparison of mercury deposition from current anthropogenic mercury emission inventories. *Environ. Sci. Technol.* **2016**, *50*, 5154–5162. [CrossRef]

11.　De Simone, F.; Artaxo, P.; Bencardino, M.; Cinnirella, S.; Carbone, F.; D'Amore, F.; Dommergue, A.; Feng, X.B.; Gencarelli, C.N.; Hedgecock, I.M.; et al. Particulate-phase mercury emissions from biomass burning and impact on resulting deposition: a modelling assessment. *Atmos. Chem. Phys.* **2017**, *17*, 1881–1899. [CrossRef] [PubMed]

12. Lindberg, S.; Bullock, R.; Ebinghaus, R.; Engstrom, D.; Feng, X.; Fitzgerald, W.; Pirrone, N.; Prestbo, E.; Seigneur, C. A synthesis of progress and uncertainties in attributing the sources of mercury in deposition. *Ambio* **2007**, *36*, 19–32. [CrossRef]

13. Jung, G.; Hedgecock, I.M.; Pirrone, N. ECHMERIT v1.0—A new global fully coupled mercury-chemistry and transport model. *Geosci. Model Dev.* **2009**, *2*, 175–195. [CrossRef]

14. De Simone, F.; Gencarelli, C.; Hedgecock, I.; Pirrone, N. Global atmospheric cycle of mercury: a model study on the impact of oxidation mechanisms. *Environ. Sci. Pollut. Res.* **2014**, *21*, 4110–4123. [CrossRef] [PubMed]

15. Holden, P.B.; Edwards, N.R.; Garthwaite, P.H.; Fraedrich, K.; Lunkeit, F.; Kirk, E.; Labriet, M.; Kanudia, A.; Babonneau, F. PLASIM-ENTSem v1.0: A spatio-temporal emulator of future climate change for impacts assessment. *Geosci. Model Dev.* **2014**, *7*, 433–451. [CrossRef]

16. Castruccio, S.; McInerney, D.J.; Stein, M.L.; Liu Crouch, F.; Jacob, R.L.; Moyer, E.J. Statistical emulation of climate model projections based on precomputed GCM runs. *J. Clim.* **2014**, *27*, 1829–1844. [CrossRef]

17. Xing, J.; Ding, D.; Wang, S.; Zhao, B.; Jang, C.; Wu, W.; Zhang, F.; Zhu, Y.; Hao, J. Quantification of the enhanced effectiveness of NO x control from simultaneous reductions of VOC and NH 3 for reducing air pollution in the Beijing–Tianjin–Hebei region, China. *Atmos. Chem. Phys.* **2018**, *18*, 7799–7814. [CrossRef]

18. Xing, J.; Zheng, S.; Ding, D.; Kelly, J.T.; Wang, S.; Li, S.; Qin, T.; Ma, M.; Dong, Z.; Jang, C.J.; et al. Deep learning for prediction of the air quality response to emission changes. *Environ. Sci. Technol.* **2020**, *54*, 8589–8600. [CrossRef]

19. Beddows, A.V.; Kitwiroon, N.; Williams, M.L.; Beevers, S.D. Emulation and sensitivity analysis of the community multiscale air quality model for a UK Ozone pollution episode. *Environ. Sci. Technol.* **2017**, *51*, 6229–6236. [CrossRef]

20. Gustin, M.S.; Bank, M.S.; Bishop, K.; Bowman, K.; Branfireun, B.; Chételat, J.; Eckley, C.S.; Hammerschmidt, C.R.; Lamborg, C.; Lyman, S.; et al. Mercury biogeochemical cycling: A synthesis of recent scientific advances. *Sci. Total. Environ.* **2020**, *737*, 139619. [CrossRef]

21. AMAP/UNEP. *Technical Background Report for the Global Mercury Assessment 2013*; Technical Report; Arctic Monitoring and Assessment Programme: Oslo, Norway; UNEP ChemicalsBranch: Geneva, Switzerland, 2013.

22. Muntean, M.; Janssens-Maenhout, G.; Song, S.; Selin, N.E.; Olivier, J.G.; Guizzardi, D.; Maas, R.; Dentener, F. Trend analysis from 1970 to 2008 and model evaluation of {EDGARv4} global gridded anthropogenic mercury emissions. *Sci. Total. Environ.* **2014**, *494–495*, 337–350. [CrossRef]

23. Streets, D.G.; Zhang, Q.; Wu, Y. Projections of Global Mercury Emissions in 2050. *Environ. Sci. Technol.* **2009**, *43*, 2983–2988. [CrossRef] [PubMed]

24. Corbitt, E.S.; Jacob, D.J.; Holmes, C.D.; Streets, D.G.; Sunderland, E.M. Global source–receptor relationships for mercury deposition under present-day and 2050 emissions scenarios. *Environ. Sci. Technol.* **2011**, *45*, 10477–10484. [CrossRef] [PubMed]

25. Climate Data Operators. Max-Plank Institute fur Meteorologie, 2014. Available online: https://code.zmaw. de/projects/cdo (accessed on 23 February 2015).

26. Simpson, D.; Benedictow, A.; Berge, H.; Bergström, R.; Emberson, L.D.; Fagerli, H.; Flechard, C.R.; Hayman, G.D.; Gauss, M.; Jonson, J.E.; et al. *The EMEP MSC-W Chemical Transport Model-Technical Description*; Copernicus: Göttingen, Germany, 2012.

27. Emmons, L.K.; Walters, S.; Hess, P.G.; Lamarque, J.F.; Pfister, G.G.; Fillmore, D.; Granier, C.; Guenther, A.; Kinnison, D.; Laepple, T.; et al. Description and evaluation of the Model for Ozone and Related chemical Tracers, version 4 (MOZART-4). *Geosci. Model Dev.* **2010**, *3*, 43–67. [CrossRef]

28. Hurrell, J.; National Center for Atmospheric Research Staff (Eds.) The Climate Data Guide: Hurrell North Atlantic Oscillation (NAO) Index (Station-Based). 2020. Available online: https://climatedataguide.ucar. edu/climate-data/hurrell-north-atlantic-oscillation-nao-index-station-based (accessed on 24 April 2020).

29. National Center for Atmospheric Research Staff (Ed.)The Climate Data Guide: Multivariate ENSO Index. 2019. Available online: https://climatedataguide.ucar.edu/climate-data/multivariate-enso-index (accessed on 15 July 2019).

30. Hynes, A.J.; Donohoue, D.L.; Goodsite, M.E.; Hedgecock, I.M. Our current understanding of major chemical and physical processes affecting mercury dynamics in the atmosphere and at the air-water/terrestrial interfaces. In *Mercury Fate and Transport in the Global Atmosphere: Emissions, Measurements and Models*; Pirrone, N., Mason, R.P., Eds.; Springer: New York, NY, USA, 2009; Chapter 14; pp. 427–457.

31. Subir, M.; Ariya, P.A.; Dastoor, A.P. A review of uncertainties in atmospheric modeling of mercury chemistry I. Uncertainties in existing kinetic parameters—Fundamental limitations and the importance of heterogeneous chemistry. *Atmos. Environ.* **2011**, *45*, 5664–5676. [CrossRef]
32. Subir, M.; Ariya, P.A.; Dastoor, A.P. A review of the sources of uncertainties in atmospheric mercury modeling II. Mercury surface and heterogeneous chemistry—A missing link. *Atmos. Environ.* **2012**, *46*, 1–10. [CrossRef]
33. Yang, X.; Cox, R.A.; Warwick, N.J.; Pyle, J.A.; Carver, G.D.; O'Connor, F.M.; Savage, N.H. Tropospheric bromine chemistry and its impacts on ozone: A model study. *J. Geophys. Res. Atmos.* **2005**, *110*, 1984–2012. [CrossRef]
34. Yang, X.; Pyle, J.A.; Cox, R.A.; Theys, N.; Van Roozendael, M. Snow-sourced bromine and its implications for polar tropospheric ozone. *Atmos. Chem. Phys.* **2010**, *10*, 7763–7773. [CrossRef]
35. Mudelsee, M. *Climate Time Series Analysis: Classical Statistical and Bootstrap Methods*; Springer International Publishing: Geneva, Switzerland, 2014.
36. Selin, N.E. Global change and mercury cycling: Challenges for implementing a global mercury treaty. *Environ. Toxicol. Chem.* **2014**, *33*, 1202–1210. [CrossRef]

Sample Availability: The HERMES CTM emulator is provided as a spreadsheet within the Supplementary Information.